# Localized corrosion of UNS A95052 aluminum alloy for application in multi-effect desalinator plants

Dannisa R. Chalfoun,[*,**], Mariano A. Kappes,[*,**,***,‡] Mauricio Chocrón,[***] and Raul B. Rebak[****]

**ARTICLE INFO**

*Article history:*

Received Day Month Year (This style is Article History and Keywords)
Accepted Day Month Year
Available Day Month Year

*Keywords:*

aluminum alloys, crevice corrosion, pitting corrosion, repassivation potential.

* Instituto Sabato, UNSAM/CNEA, Av. Gral. Paz 1499, San Martín, Buenos Aires, B1650KNA, Argentina

** National Scientific and Technical Research Council, Godoy Cruz 2290, Autonomous City of Buenos Aires, C1425FQB, Argentina

*** National Commission of Atomic Energy of Argentina, Av. Gral. Paz 1499, San Martín, Buenos Aires, B1650KNA, Argentina.

**** GE Global Research, 1 Research Circle, Niskayuna, NY 12309, USA

‡Corresponding author: +54-11-6772-7353.
Email: kappes@cnea.gov.ar

**ABSTRACT**

Aluminum alloy UNS A95052 (AA 5052) results very attractive for desalination applications due to its good corrosion resistance in seawater at temperatures up to 125ºC, low cost, good thermal conductivity, and non-toxicity of its corrosion products. The pitting corrosion potential, $E_{pit}$, and the pit repassivation potential, $E_{r,\,pit}$, of AA 5052 were measured in deaerated 65,000 ppm sodium chloride (NaCl) solutions at 30, 60 and 85ºC. $E_{pit}$ decreased with temperature, in accord with literature results. $E_{r,\,pit}$ was a function of anodic charge passed during pit growth stage. A complete evaluation of suitability of this alloy from a corrosion perspective requires also studies of crevice corrosion at different temperatures, considering that multi-plate designs of desalinators have metal plates in contact with rubber gaskets and seals. Cyclic potentiodynamic polarization were used to estimate crevice repassivation potentials, $E_{r,crev}$, at 30, 60 and 85ºC, in specimens with an attached rubber O-ring as a crevice former. This crevice former simulated the partially occluded geometry expected in desalination plants. Stable crevice corrosion potentials, $E_{crev}$, were similar to $E_{pit}$, and, when polarized to a similar anodic charge density, $E_{r,crev}$ were similar to $E_{r,\,pit}$. Based on this result, from a corrosion perspective, the presence of crevices in the desalination plant is not expected to present an additional risk during operation of the plant. Electrochemical tests were also performed in saturated $AlCl_3$ solutions to explain the results using Galvele's localized acidification model.

## INTRODUCTION

Seawater desalination using waste heat from nuclear or fossil power plants is an attractive alternative for the production of potable water.[1] Multi-effect desalination process (MED) relies on the evaporation of water from a thin film of seawater.[2] The heat released during condensation of distilled water on the metallic surface is transported through the thickness of the plate and used for the evaporation of water from a subsequent film of seawater, thus allowing an efficient production of distillate. Materials for use in such plants must have an adequate corrosion resistance in seawater at 70°C or higher, [1,2] depending on the design and type of plant. The formation of a continuous film of seawater and condensed water is critical to minimize precipitation of deposits and hot spots. Aluminum alloys (AA), in particular UNS A95052[(1)] (referred hereafter as AA 5052), possess several advantages for this application, including a good thermal conductivity, [3,4] high seawater corrosion resistance[4], low cost when compared to copper or titanium alloys, [5] non-toxicity of the alloy or its corrosion products,[6] and good wettability in seawater at high temperature. [3] Therefore, AA are often the chosen materials for MED applications. [1–3,6–10]

Among wrought AA alloys, non-heat-treatable 5xxx series have the highest resistance to seawater corrosion, due in part to the absence of copper as an alloying element. [4,11]. Magnesium (Mg) is the main alloying element in this series, and its equilibrium solubility at room temperature in the aluminum matrix is below 1wt% [12]. In alloys with higher content of magnesium β phase ($Mg_2Al_3$) precipitation is thermodynamically possible. However, a supersaturation of Mg is required due to kinetics constraints, and a threshold content of 3wt% of Mg is often quoted for β phase precipitation [13–15]. The threshold value might depend on details of the microstructure including amount of cold work, grain size and concentration of other alloying elements [16]. β phase is anodic with respect to the matrix, [13,17,18] and its grain boundary precipitation can lead to intergranular corrosion (IGC) and stress corrosion cracking (SCC) problems [13,14,16,19–21]. Those problems are typically observed in alloys with magnesium content above about 4 wt.%. Below this threshold value in Mg concentration, specimens subjected to a sensitizing heat treatment (150°C for seven days) exhibited a negligible weight loss in the concentrated nitric acid immersion test[21]. Hence, for AA 5052 with a Mg content around 2.5 wt.%, absence of or a scarce amount of β phase in AA5052 is expected, which results in its high resistance to intergranular corrosion and intergranular SCC [12]. Specimens of AA 5052 exposed to 70°C for 30 months exhibited an extremely low corrosion rate of 4 mg/cm$^2$ in concentrated nitric acid [22], which is more than one order of magnitude lower that for alloy 5083 (UNS A95083, with 4.85 wt.% Mg). However, some unusual cases of intergranular attack of alloy 5052 were reported [4], and they are probably related to presence of cold work. In particular, in desalination service, IGC was observed in the area of tubes rolled into the tube sheet, at a service temperature above 104°C [23].

While resistance to IGC of alloy 5052 is expected to be high under most conditions, the presence of chlorides ($Cl^-$) in feed seawater can lead to pitting corrosion of the AA 5052 alloy. [6,9,24,25] A common measure of resistance to pitting corrosion is the pitting potential, $E_{pit}$, [26–29] defined as the potential above which corrosion pits are stable. [26] $E_{pit}$ of aluminum alloys in sodium chloride solutions decreases as the

[(1)]UNS numbers are listed in Metals and Alloys in the Unified Numbering System, published by the Society of Automotive Engineers (SAE International) and cosponsored by ASTM International.

temperature [6,30,31] and chloride concentration increases. [28,32] During the operation of the desalinator, the material can experience exposure to environments with chloride concentrations above that of seawater (~20,000 ppm $Cl^-$) at temperatures of 70°C or higher, therefore promoting pit growth. Stable corrosion pits can continue to grow even if polarized below $E_{pit}$,[29,32] and eventually they can repassivate if polarized below the repassivation potential or protection potential, $E_{r,pit}$. [26,33] For potential values between the $E_{r,pit}$ and $E_{pit}$,, metastable pits can nucleate and stable pits can grow, therefore, a conservative criteria for preventing pitting damage is that the steady state corrosion potential, $E_{corr}$, fulfills $E_{corr}<E_{r,pit}$. [34]

Operation of desalination plants usually involves deaeration of seawater to minimize problems associated with non-condensable gases. [2] Bonewitz[6] showed that, for aluminum alloy AA 5052 in deaerated synthetic seawater in the temperature range between 25 and 100°C, $E_{r,pit} - E_{corr} > 100$ mV. This difference guarantees that in case of pit initiation due to possible excursions of $E_{corr}$ (for example, due to ingress of oxygen), any corrosion pit nucleated during the oxygen ingress transient will repassivate once the system returns to normal steady state conditions. In other words, based on this data, pitting corrosion should not be a problem during steady state deaerated operation of the desalination plant. On the other hand, in presence of heavy metal cations like $Cu^{++}$ [24,28] $E_{corr}$ could increase and stabilize at $E_{pit}$ value of aluminum, [28,35] and this caused pitting problems in service in some aluminum desalination plants. [6,36] It is recommended[11,36,37] to avoid the use of copper alloys upstream the aluminum desalinator to prevent pitting corrosion and/or galvanic corrosion.

While pitting corrosion can be controlled by removing oxygen from the seawater feed and by minimizing the presence of heavy ions that shifts $E_{corr}$ to nobler values, the possibility of crevice corrosion has to be evaluated[19]. Desalination plants, and in particular those of the multieffect type, usually have polymeric seals or gaskets in contact with the aluminum alloy plates or tubes,[2] which could act as initiation sites for crevice corrosion. Crevice corrosion of AA 5052 was studied in seawater with artificial crevice formers at room temperature.[35] For a 3.0 wt% NaCl solution, the crevice repassivation potential, $E_{r,crev}$, was -0.960 $V_{SCE}$, [35] which is below $E_{corr}$ of aluminum in synthetic seawater at room temperature. No studies of the dependence of $E_{r,crev}$ of AA 5052 with temperature were found in the literature; however, it is likely that the $E_{r,crev}$ should decrease with increasing temperature, in a similar fashion as $E_{r,pit}$ and $E_{r,crev}$ of *UNS* A91100[34] or $E_{r,pit}$ of AA 5052. [6] Crevice corrosion was observed during potentiostatic laboratory tests, where UNS A95082 was polarized to a potential slightly above $E_{r,crev}$ measured in 3.0 wt% NaCl. [35] In laboratory tests, the potentiostat can supply all the current necessary for the crevice to grow. On the other hand, the growth of crevices under open circuit conditions in seawater are limited by the rate at which oxygen[38] and water can reduce on the free surface, and therefore can control the dissolution of Al.

Despite predictions of laboratory tests reported by Furuya and Soga[35], some authors have stated that the crevice corrosion of aluminum alloys in neutral chloride solutions at room temperature is "not a concern for industrial applications", [39] is "not as destructive and common as crevice corrosion of steels and titanium"[40] and is an effect that weakens with full immersion in seawater, because pitting in the boldly exposed surface becomes comparable to the attack in the crevice. [41] In this regard, field exposures of UNS A91050A, UNS A95083 and UNS A96082 aluminum alloys with artificial crevice formers to aerated seawater did not show evidence of crevice corrosion. [42] Similar results were obtained for Al-Cr, Al-Mg and Al-Mg-Cr alloys. [43] However, all those results addressed corrosion resistance in chlorides solutions at room temperature, while the possibility of crevice corrosion occurrence at higher temperatures was not studied.

The crevice corrosion of alloy AA 5052 has not been studied at temperatures higher than room temperature. Those studies are critical for multi-plate multi-effect desalinator (MP-MED) plants based on multi-plate geometry, where elastomeric seals required for preventing leaks and oxygen ingress from the environment create artificial occluded regions or crevices in contact with the metal surface. Furthermore, according to a recent study[30] the structure of passive films on pure aluminum changes at a temperature of 40°C and above, and the effect this oxide film change might have on crevice corrosion resistance of AA was not studied until now. Therefore, the main objective of this work is to measure the $E_{crev}$ and $E_{r,crev}$ of AA5052 at temperatures and chloride concentration relevant to desalination service , in order to predict resistance of the alloy to crevice corrosion.

## EXPERIMENTAL

The parent material was a commercial plate of AA 5052 H32 with a nominal chemical composition as detailed in Table 1. The letter H in the suffix indicated the alloy was strain hardened, the number two specifies the amount of strain hardening present (in an increasing scale from 0 to 8) and the number 3 indicates that the alloy was stabilized at 120-175°C to prevent softening after strain hardening [14]. Specimens were cut from the parent plate and ground to 600 grit SiC paper in ethanol, to minimize pitting during the preliminary electrode or specimen preparation. A three-electrode cell with nitrogen deaeration capabilities was used for all the experiments. A saturated calomel electrode (SCE) ($E_{SCE}$ = 0.241 $V_{NHE}$) was used to measure the potentials via a Luggin capillary, and a graphite bar served as the counter electrode. The reference electrode was connected to the Luggin capillary via a water refrigerated port, kept at room temperature. All potentials in this work are reported vs. SCE at 25°C.

No additional stirring of the testing electrolyte was used during the corrosion tests other than the mild agitation provided by the nitrogen gas bubbler. Flow regime and flow velocity are important parameters that control desalinator performance[3]. However, stagnant solutions favor the occurrence of localized forms of corrosion like pitting and crevice corrosion. Hence the approach followed here despite limited is conservative. In all the experiments, seawater was simulated by NaCl solutions that were made from analytical grade NaCl and ultrapure water (resistivity of 18.2 MΩ·cm at 25ºC). The NaCl concentration was 65,000 ppm or 39,000 ppm $Cl^-$ concentration. This more concentrated salt solution addressed the increase in salt concentration above normal seawater content (~35,000 ppm NaCl), because of the water evaporation that can occur inside the desalination plant during its operation. The temperature was kept constant during the experiments using a thermostatisized bath, set at either 30°C, 60°C or 85°C. A condenser was used to prevent water vapor being carried away by the nitrogen used to remove the oxygen from the test solution. All the experiments were repeated at least two times for each chloride concentration and temperature. A Stern-Makrides[44] electrode assembly was used for all the corrosion experiments.

The specimens for pitting corrosion experiments had an exposed area of about 15 $cm^2$ and were partially immersed in the solution to avoid undesired crevices due to gasket-metal solution exposure. The solution was deaerated for 1 h prior to starting the experiments. At this point, the working electrode or test specimen was introduced in the cell and $E_{corr}$ was measured for 1 h. For pitting corrosion experiments, the working electrode was potentiodynamically polarized from 20 mV below $E_{corr}$ in the noble direction, at a scanning rate of 0.167 mV/s, until an anodic current of 3 mA was attained. Some experiments were performed where this maximum current was either 0.5, 45 mA or 250 mA. After reaching the maximum set anodic current, the potential was scanned in the active direction, which eventually caused repassivation

of corrosion pits formed in the anodic scan. $E_{pit}$ and $E_{r,\,pit}$, were obtained from inspection of the E-I curves, as the point where a sudden anodic increase in current occurred in the forward direction and as the point where the reverse scan crossed the forward scan, respectively. This definition of $E_{r,\,pit}$ is equivalent to stating that it is the potential where the current attains the passive current density measured in the forward scan[45]. When the backwards scan did not intersect with the forward scan, (see for example the curves for 45 mA or 250 mA in figure 2), the repassivation potential was estimated as the potential where the backward scan intersected with the extrapolation of the passive current density below the corrosion potential.

The specimens for crevice corrosion tests had an exposed area of approximately 10 $cm^2$. A 7 mm diameter hole allowed insertion of a titanium bolt that was used to attach a crevice former. This bolt was wrapped with polytetrafluoroethylene tape to prevent galvanic contact with the aluminum working electrode, which also was verified previous to each test with a multimeter. The crevice former consisted of a rubber O-ring, Figure 1. This non-standardized geometry is expected to be like the one experienced by the plates in the MP-MEE plant, which will be in contact with rubber seals or gaskets. The titanium nut and bolt were tightened until reaching a preset deformation of the O-ring, measured with a caliper to guarantee reproducibility in the crevice geometry. The open circuit potential pre-exposure time and cyclic polarization parameters were the same than for the specimens with no crevice formers, and $E_{crev}$ and $E_{r,\,crev}$, were similarly obtained by inspection of the E-I curves.

$E_{corr}$ measurements and anodic polarization experiments were performed in samples without crevice formers in a saturated $AlCl_3$ solution (45.1 gr $AlCl_3$/100 gr $H_2O$[46]), which simulates the expected solution inside aluminum corrosion pits in chloride bearing solutions.[47] $E_{corr}$ in the deaerated solution was measured during 1 h, and then a potential scan in the anodic direction was performed.

Finally, specimens with O-ring crevice formers were immersed at $E_{corr}$ under deaerated conditions in 65,000 ppm NaCl solution for 72 h at different temperatures, to estimate steady state $E_{corr}$ and predict the performance of the material in the desalination plant. Some experiments were repeated with an intentional 5 ppm addition of $Cu^{++}$ (added as $CuCl_2{\cdot}2H_2O$) and with air bubbling, thus simulating possible plant operation runs that could occur in case of improper selection of materials, for example, copper or brass pipes upstream the desalinator. [28]

All tested specimens were observed under the optical or scanning electron microscope (SEM) to characterize the morphology of the attack.

# RESULTS AND DISCUSSION

### *Pitting and crevice corrosion experiments in 65,000 ppm NaCl solution*

Figure 2 shows cyclic potentiodynamic curves obtained for AA5052 in 65,000 ppm NaCl solution at 30°C, for specimens without crevice former. The maximum anodic current was set to either 250 mA, 45 mA, 3 mA or 0.5 mA. The potential at open circuit conditions exhibited a variation of ± 50 mV. At this potential and in neutral environments, the aluminum alloy exhibits passive behavior, and $E_{corr}$ is determined by the intersection of the anodic and cathodic branch, both of which have low slopes[34]. Therefore, experimental variations in the sample and environment, including, thickness of the air grown passive layer, exposed area of intermetallic particles, and the amount of oxygen remnant in solution after deaeration will affect the parameters of anodic and cathodic curves and given the low slope values they could have a big effect on the $E_{corr}$ values measured after the first hour of immersion. At potentials above $E_{corr}$, all the curves show a passive range followed by a breakdown potential, $E_{pit}$, with a sharp increase in current and in the reverse scan, an inflexion point is apparent for all four measurements, which occurs at potentials close to $E_{pit}$. This behavior was previously observed in aluminum alloys exposed to sodium chloride solutions and the inflexion point was named the pit transition potential, $E_{ptp}$,[48] (Figure 2). At potentials lower than $E_{ptp}$, the current density still decreases with the potential but at a much lower rate, until eventually the reverse scan intersects with the forward scan, at the crossover potential, a conventional measure of $E_{r,pit}$.[48] $E_{ptp}$ does not vary with total anodic charge as markedly as $E_{r,pit}$, (Figure 3), and the current density at $E_{ptp}$ increased with maximum current density reached during the forward scan, (Figure 2), both statements in accord with literature results. [48–50]

Corrosion pits are expected to grow deeper as the total charge density increases; therefore, Figure 2 results also suggest that $E_{ptp}$ is almost independent of pit depth. Some authors have stated that $E_{ptp}$ is a protection or repassivation potential, [31,51] thus leading to the conclusion that pit repassivation is independent of pit depth, in contrast to the case for stainless steels.[52–54] However, in the more conservative approach[48] selected for this work, the crossover potential was identified with pit repassivation. Another reason that discourages the identification of $E_{ptp}$ with a repassivation potential is that, under certain experimental conditions, like the curve for 250 mA in figure 2, $E_{ptp}$ was higher than $E_{pit}$. Moore et al.[50], working with a Al–Li–Mg alloy in chloride solutions, also concluded that $E_{ptp}$ can be higher than $E_{pit}$. Furthermore, the current density at potentials below $E_{ptp}$ was on the order of 100 $\mu A/cm^2$ for the 250 mA curve, which is more than two orders of magnitude above the passive current density measured in the forward scan, Figure 2. Given those considerations, $E_{ptp}$ cannot be related to a repassivation process based on the currently accepted pit mechanism [29,54]. There are various explanations for the higher current density at reverse vs. forward scans when the potential is lower than $E_{ptp}$. Those include, acid build up at the interface,[55] incomplete repassivation of deep pits,[48] or propagation of tunnels inside pits,[50,56,57] which are a more occluded, microscopic form of attack that propagates unidimensionally (i.e., a smaller pit propagating inside a larger pit).

Cyclic polarization curves of AA 5052 in NaCl solution at 60°C are presented in Figure 4. The specimens polarized without and with the crevice former showed in Figure 1 exhibited a breakdown potential near -800 $mV_{SCE}$, and a hysteresis loop, characteristic of localized corrosion processes.[29,52,53] Specimens with and without crevice formers exhibited similar values of breakdown and repassivation potentials. The specimens were polarized to the same final anodic current (3 mA), but the specimens with the crevice former were normalized by the boldly exposed area, hence the difference in maximum current density.

Figure 5 summarizes results obtained for AA5052 in 65,000 ppm NaCl at 30, 60 and 85°C. All the experiments were at least replicated twice, and mean values are reported, with error bars representing standard deviations. $E_{pit}$, $E_{r,\,pit}$, $E_{crev}$ and $E_{r,\,crev}$ decreased with a similar slope with an increase in the temperature, similar to what was shown by Bonewitz[6,58] for $E_{r,\,pit}$ of various aluminum alloys, including AA 5052. The presence of the crevice former did not affect the breakdown potential significantly, as $E_{pit}$ and $E_{crev}$ were similar for the three temperatures studied. Differences between $E_{r,\,pit}$ and $E_{r,\,crev}$ were within 50 mV for the three temperatures studied.

Current $E_{r,\,pit}$ values for AA5052 were about 100 mV lower than $E_{r,\,pit}$ values reported by Bonewitz[6] for the same alloy. The higher chloride

concentration used in this work could explain only a fraction of this difference. According to Galvele´s localized acidification mechanism[29], there is a 59 mV decrease in $E_{r,pit}$ for every tenfold increase in chloride concentration at room temperature. Hence, considering Bonewitz[6] measurements were made in synthetic sea water, the difference in chloride concentration should account for a difference in 16, 18 and 20 mV in $E_{r,pit}$ at 30, 60 and 85°C. Differences in material composition and microstructures might contribute to this difference. Bonewitz[6] stated that $E_{r,pit}$ values for AA5052 alloy were not a function of anodic charge passed in the tests, which is in contrast to the results presented here, (Figure 3), where independence of anodic charge is a property of $E_{ptp}$, not $E_{r,pit}$.

Figure 6 shows SEM micrographs obtained after performing cyclic potentiodynamic tests with crevice formers. At 30°C, corrosion pits nucleated and grew preferentially at the crevice former boundary with the electrolyte, and a higher magnification image (Figure 7, left) shows that corrosion pits had crystallographic etch patterns.[59] At 60°C a high density of pits is evident near the crevice former (Figure 6, center) and the crevice mouth was occluded with corrosion products, (Figure 7), center. Corrosion products with cracked mud appearance are seen below the crevice former at 60 and 85°C, (Figure 7), center and right. At 85°C the corrosion pits had a similar appearance than at 30°C, with crystallographic etch patterns. No instances of intergranular corrosion were observed under the conditions studied.

Figure 8 (left) shows the time evolution of $E_{corr}$ in saturated $AlCl_3$ solution during the first hour of immersion. For all temperatures, $E_{corr}$ rapidly stabilized to a steady state value, which decreased with increasing temperature. $E_{corr}$ in this solution is compared with stable growth and repassivation potentials in Figure 5. The aluminum alloy anodic dissolution reaction in saturated $AlCl_3$ exhibited an active dissolution controlled behavior with appreciable ohmic potential drop at current densities above 1 mA/cm$^2$, with no indication of passivity or salt film precipitation, Figure 8 (right). The absence of salt film precipitation could be related to the solution mixing created by hydrogen bubbles. [60] According to Beck, [61] this solution should have a pH near -0.25. It is likely that both, chlorides and low pH, contributed to the absence of passivity in this solution, since a pure aluminum specimen polarized in 1 M HCl (pH=0) had a passivity range extending from -0.9 $V_{SCE}$ to -0.8 $V_{SCE}$, [62] exhibiting a breakdown potential at -0.8 $V_{SCE}$. In less concentrated $AlCl_3$ ($3\cdot10^{-3}$, 0.03 and 1 M) solutions, other authors[59] also reported a passive range followed by a breakdown potential, which decreased with increasing the concentration of $AlCl_3$.

The decrease in $E_{corr}$ in $AlCl_3$ with temperature can explain the dependence of $E_{pit}$ and $E_{crev}$ with temperature, Figure 5. According to Galvele's[29] localized acidification model $E_{pit}$, can be modeled according to Equation 1:

$$E_{pit} = E_{corr}^{*} + \eta + \phi \qquad (1)$$

Where $E_{corr}^{*}$ is the corrosion potential in the solution that simulates the pit solution (saturated $AlCl_3$), $\eta$ is the overpotential required to maintain the critical $x\cdot i$ value and $\phi$ is the ohmic drop induced by electromigration of charged species to the bottom of the pit. The slope of $E_{pit}$ and $E_{crev}$ vs. T is like the slope of $E_{corr}$ vs. T in $AlCl_3$, thus suggesting that contributions of the $\eta + \phi$ terms are similar for the three temperatures studied, Figure 5.

The critical $x\cdot i$[29] value allows to maintain a critical acidification of the pit or crevice by hydrolysis of metallic cations, where x is the characteristic depth of the defect (i.e. pit) and i is the anodic current density at the bottom of the pit. While crevices should have a considerable larger x value than pits, therefore leading to a required lower critical current density and in turn a lower $E_{crev}$ and $E_{r,crev}$, Figure 6 shows that in this system, crevice attack occurred close to the boundary of the crevice former, not deep underneath the crevice former. This might explain the little difference observed between $E_{pit}$ and $E_{crev}$ for the studied AA5052 specimens. Furthermore, according to Galvele[63], the difference in $E_{pit}$ and $E_{crev}$ should scale with the anodic Tafel slope values of the alloy in the simulating pit/crevice solution. The values of anodic Tafel slope lower than 50 mV in concentrated chloride solutions, Figure 8, predict similar potentials for $E_{pit}$ and $E_{crev}$ [63].

Galvele's model[29] is also useful for estimating a lower bound for both repassivation potentials.[64] As the potential is scanned in reverse, corroded pits and crevices repassivate at a potential lower than $E_{pit}$ and $E_{crev}$, which is related to the fact that the depth x increased during the forward or constant current growth periods. $E_{corr}^{*}$ is the minimum possible value for $E_{r,pit}$ and $E_{r,crev}$, so it could be used as a conservative lower bound. $E_{r,crev}$ at 85°C, Figure 5, and $E_{r,pit}$ at 30°C when the maximum applied current density was 600 mC/cm$^2$ or higher, Figure 3, were lower than the corresponding $E_{corr}$ in saturated $AlCl_3$, Figure 8. Therefore, the saturated $AlCl_3$ solution could be a more aggressive solution than the one present inside pits and crevices. Some authors claim that the pH inside aluminum pits and crevices should be near 3 or 4. [38,40,65–70] According to Beck,[61] the pH of saturated $AlCl_3$ is near -0.25, while the predicted $AlCl_3$ concentration to yield a solution with pH between 3 and 4 is $3\cdot10^{-3}$ M to 0.3 M. Polarization curves presented by Baumgartner and Kaesche[59] showed that for $AlCl_3$ concentrations between $3\cdot10^{-3}$ M to 1 M, $E_{corr}$ at room temperature did not vary appreciably with $AlCl_3$ concentration, rather, it remained near -0.940 $V_{SCE}$, which is lower than the value measured here in saturated $AlCl_3$ solution, Figure 8. However, unlike the tests reported in this work in saturated $AlCl_3$ solution, polarization curves reported by Baumgartner and Kaesche[59] showed a passive behavior followed by a breakdown potential. Hence, those results[59] cannot represent the exact electrochemical behavior of aluminum at pit bottoms.

### *Open circuit corrosion potentials in deaerated 65,000 ppm NaCl solution*

$E_{corr}$ measured in 65,000 ppm NaCl are presented in Figure 5. Vertical hatched bars were chosen to represent the fluctuation of $E_{corr}$ measured during a 72 h immersion period. Similar to results presented by Bonewitz,[6] $E_{corr}$ in deaerated NaCl reached potentials as high as ~ –900 $mV_{SCE}$. Temperature did not have a clear effect in $E_{corr}$, which could be related to the fact that temperature affects many of the parameters that control $E_{corr}$. The kinetics of the hydrogen evolution reaction should increase with temperature[71]. However, this shift of corrosion potential in the noble direction could be masked by the change in kinetics of anodic reactions, for instance, the passive current density of aluminum alloys in chloride solutions increases with temperature[30]. In contrast, in solutions without forced de-aeration, the decreasing solubility of oxygen with temperature[25] might explain the decrease in corrosion potential, as showed by Soltis et al. [30] It is shown in figure 5 that $E_{pit}$, $E_{r,pit}$, $E_{crev}$ and $E_{r,crev}$ decreased with temperature, thus favoring localized corrosion. While Bonewitz predicted resistance to pitting corrosion based on $E_{corr}<E_{r,pit}$ criterion, significantly lower $E_{r,crev}$ and $E_{r,pit}$ were measured in this work, thus, both crevice and pitting corrosion could in fact affect the integrity of the desalinator, especially at 30 and 85°C. Care should be taken to prevent any excursion in potential that could lead to pitting and crevice corrosion initiation, for example, via oxygen or copper ion contamination. Considering that $E_{r,pit}$ and $E_{r,crev}$ measured in this work were lower than steady state $E_{corr}$ in deaerated conditions, localized corrosion in pits and crevices might continue if initiated during higher potential excursions. Moreover, $E_{r,pit}$ was found to be a function of pit growth in

this work, Figures 2 and 3. $E_{corr}$ at 30°C is lower than the $E_{r,pit}$ when the pits grew up to 20 mC/cm$^2$. Observation of specimens in the optical microscope after a 72 h exposure at $E_{corr}$ revealed some incipient pits, localized uniformly in the specimen. Breakdown, $E_{pit}$ and $E_{crev,}$ and repassivation potentials, $E_{r,pit}$ and $E_{r,crev}$, reported in this work correspond to stable growth and repassivation of stable pits or crevices in the aluminum matrix. However, aluminum alloys typically contain constituent particles due to the presence of alloying elements or impurities. A possible second phase present in this alloy is $Mg_2Si$,[72] which can dissolve actively (i.e. without passivation) at potentials of ~ -900 $mV_{SCE}$. [73] Alternatively, iron rich particles like $Al_3Fe$[72] have an $E_{corr}$ more noble than the matrix[73] and can promote dissolution of the surrounding matrix.[72] The incipient pits observed in the specimens exposed to deaerated seawater could be associated with such iron rich particles.

***Corrosion behavior in aerated 65,000 ppm NaCl solution with 5 ppm $Cu^{++}$***

$Cu^{++}$ can reduce on the aluminum alloy surface yielding metallic Cu, thus providing a surface where oxygen can reduce efficiently.[28] As a consequence, $E_{corr}$ of the alloy increases up to the breakdown $E_{pit}$. [28,35] In those tests contaminated with cupric ions, the corrosion potential of the specimens increased to -765 $mV_{SCE}$, -791 $mV_{SCE}$ and -827 $mV_{SCE}$ when they were exposed to 30, 60 and 85°C, respectively, Figure 5. In the three cases the maximum potential reached was close to $E_{crev}$, Figure 5. After a 72 h period at $E_{corr}$, deep trenches were observed under the O-ring, Figure 9, suggesting severe crevice corrosion attack under the crevice former. While constituent particles (whose typical size is between 0.5 – 10 μm[14]) might have a role in the initiation of the attack, notice that the size of the dissolved region has a size on the order of 200 μm. Therefore, it is likely that most of them fell off or were completely dissolved at this stage of the attack. Deposits with cracked mud appearance were detected near those trenches, and a higher magnification of the crevice attacked zone revealed crystallographic type of features as previously shown for the potentiodynamic tests, Figure 7. While some pits were also observed in the boldly exposed surface, the depth of the attack was largest under the O-ring and at the water-vapor interface. Considering that due to the operation of the desalinator the aluminum alloy surface will be in contact with both O-rings and partially immersed areas, strict limits for $Cu^{++}$ (and any other oxidant species like $Fe^{++}$ or $Fe^{+++}$) are needed on the seawater feed. An alternative to reduce the content of those aggressive species in the seawater is forcing the feed water through a heavy ion trap[74] filled with aluminum scrap. Several authors point that $Cu^{++}$ [8,11] concentrations below 40 ppb do not cause aluminum pitting, and considering that pit and crevice have similar stable growth and repassivation potentials, the same limit may be adopted for preventing crevice attack.

# CONCLUSIONS

The localized corrosion of AA 5052 in chloride solutions was studied using specimens with and without crevice formers, which simulate the plate geometry of multi-plate multi-effect evaporator (MP-MEE) in desalination plants. The following conclusions were drawn on the results presented herein:

- $E_{crev}$ and $E_{r,crev}$, measured in cyclic potentiodynamic tests, were similar to $E_{pit}$ and $E_{r,pit}$ measured under the same experimental conditions. Therefore, this laboratory test predicts that during normal operation the presence of elastomeric seals will not increase the risk for the desalinator plates integrity.
- $E_{pit}$, $E_{r,pit,}$ $E_{crev}$ and $E_{r,crev}$ decreased with temperature, with a slope similar to the one exhibited by the $E_{corr}$ of AA5052 in saturated $AlCl_3$ solutions.
- In presence of crevice formers, pits and localized attack nucleated preferentially at the mouth of the surface partially occluded by the crevice material, as observed in potentiodynamic tests and open circuit exposures in solutions containing $Cu^{++}$ ions. This could explain the similarity in breakdown and repassivation potentials measured in potentiodynamic tests in specimens with and without crevice formers.
- $E_{r,pit}$ decreased with an increase in the maximum current density reached in the forward potential scan. No lower bound $E_{r,pit}$ was found, for values of anodic charge density between 0.004 and 20 C/cm$^2$.
- $E_{ptp}$ was independent of the anodic charge circulated in the forward potential scan. Current density below this potential can be more than two orders of magnitude higher than passive current density, hence, it cannot represent a repassivation potential.
- $E_{corr}$ measured during a 72 h period in deaerated 65,000 ppm NaCl solutions were near or higher than $E_{r,pit}$ and $E_{r,crev}$. Therefore, in order to minimize the risk of onset of pitting and/or crevice corrosion during desalinators operation, care must be taken to maintain the feed-water free from oxygen and heavy metal ions contamination.

# AKNOWLEDGEMENTS

This work is part of a Coordinated Research Project financed by the International Atomic Energy Agency (IAEA), CRP code 18470, contract number I35005.

***References***

1. S. Nisan, G. Caruso, J.R. Humphries, G. Mini, A. Naviglio, B. Bielak, O. Asuar Alonso, N. Martins, L. Volpi, Nucl. Eng. Des. 221 (2003) 251–275. doi:10.1016/S0029-5493(02)00337-0.
2. A. Ophir, F. Lokiec, Desalination. 182 (2005) 187–198. doi:10.1016/j.desal.2005.02.026.
3. A. Stärk, K. Loisel, K. Odiot, A. Feßenbecker, A. Kempter, S. Nied, H. Glade, Desalin. Water Treat. 55 (2014) 2502–2514. doi:10.1080/19443994.2014.957919.
4. E. Ghali, Aluminum and aluminum alloys, in: R. Winston Revie (Ed.), Uhlig's Corros. Handb., 3rd ed., John Wiley & Sons, 2011: pp. 715–745.
5. W.D. Callister, D.G. Rethwisch, Fundamentals of materials science and engineering-an integrated approach, 3rd. ed, John Wiley & Sons, 2008.
6. R.A. Bonewitz, Corrosion. 29 (1973) 215–222.
7. E.D. Verink, P.F. George, Mater. Perform. 12 (1973) 26–30.
8. Z. Ahmed, Anti-Corrosion Methods Mater. 28 (1981) 4–7.
9. O.M. Lebedeva, A.H. Lebedev, M.N. Fokin, S.V. Lomakina, T.A. Severorova, B.A. Gromov, Desalination. 73 (2013) 457–458.
10. Z. Ahmed, S. Rashidi, Desalination. 44 (1983) 265–276.
11. F.L. LaQue, Ocean Eng. 1 (1969) 299–312.
12. E. H. Dix, W. A. Anderson & M. B. Shumaker, Corrosion 15 (1959) 55t–62t.
13. J. A. Lyndon, R. K. Gupta , M. A. Gibson & N. Birbilis, *Corros. Sci.* 70 (2013), 290–293.
14. I. Polmear, *Light alloys - From traditional alloys to*

*nanocrystals*, 4th ed. (Oxford, UK: Elsevier, 2006).
15. M. A. Steiner & S.R. Agnew, Corrosion 72 (2016), 169–176.
16. Zhang, R. et al., Corrosion 72 (2016), 144–159.
17. N. Birbilis & R.G. Buchheit, J. Electrochem. Soc. 152 (2005), B140–B151.
18. R.G. Buchheit, J. Electrochem. Soc. 142 (1995), 3994–3996.
19. J.N. Wanklyn, N.J.M. Wilkins, D. R. V. Silvester, C.E. Austing & P.F. Lawrence, Desalination 9 (1971), 245–258.
20. M. L. C. Lim, J. R. Scully & R. G. Kelly, Corrosion 69 (2013), 35–47.
21. R. Gupta, R. Zhang, C. Davies & N. Birbilis, Corrosion 69 (2013), 1081–1087.
22. G. Yi et al., Corrosion 72 (2015), 177–186.
23. D. A. Fauth and R. I. Lindberg. Aluminum Heat Transfer Surfaces Multistage Flash Distillation Plant, Research and development progress report No. 583, Office of Saline Water. (1970).
24. M.G.A. Khedr, M.M.H. Badran, A.A. El Azhari, Desalination. 72 (1989) 351–366.
25. S.C. Dexter, Corrosion. 36 (1980) 423–432.
26. Z. Szklarska-Smialowska, Corros. Sci. 41 (1999) 1743–1767.
27. H. Holtan, H. Sigurdsson, Werkstoffe Und Korrosion. 28 (1977) 475–477.
28. H. Bohni, H.H. Uhlig, J. Electrochem. Soc. 116 (1969) 906–910.
29. J.R. Galvele, J. Electrochem. Soc. 123 (1976) 464–474.
30. J. Soltis, N.J. Laycock, D. Krouse, Corros. Sci. 53 (2011) 7–10.
31. A. Broli, H. Holtan, Corros. Sci. 13 (1973) 237–246.
32. Z.A. Foroulis, M.J. Thubrikar, Electrochim. Acta. 21 (1976) 225–230.
33. M. Pourbaix, J. Less-Common Met. 28 (1972) 51–65.
34. N. Sridhar, C.S. Brossia, D.S. Dunn, A. Anderko, Corrosion. 60 (2004) 915–936.
35. S. Furuya, N. Soga, Corrosion. 46 (1990) 989–993.
36. R.J. Gainey, Corrosion. 17 (1961) 526t–528t.
37. S.C. Dexter, Localized corrosion of aluminum alloys for OTEC heat exchangers, Argonne National Laboratory report prepared for the U.S. Department of Energy, Argonne, Illinois, US, 1979.
38. P. Su, O.F. Devereux, Corrosion. 59 (2003) 780–789.
39. B.S. DeForce, B.A. Shaw, Documented evidence of significant metal loss in aluminum crevice corrosion, in: NACE Corrosion 2016, NACE International, Vancouver B.C., Canada, 2016.
40. K. Hebert, R. Alkire, J. Electrochem. Soc. 130 (1983) 1001–1007.
41. V.S. Sinyavskii, V.D. Kalinin, Prot. Met. 41 (2005) 317–328.
42. J.W. Oldfield, G.L. Masters, K.R. Stokes, Prediction of initiation and propagation of crevice corrosion on aluminium alloys in sea water by mathematical modelling, in: NACE Corrosion 1996, NACE International, p. Paper 512.
43. G. Venkateswaran, K.S. Venkateswarlu, E. Galow, Key Eng. Mater. 20–28 (1988) 1587–1600.
44. M. Stern, A.C. Makrides, J. Electrochem. Soc. 107 (1960) 782.
45. A.K. Mishra, G.S. Frankel, Corrosion 64 (2008): p. 836-844.
46. D.R. Lide, ed., CRC Handbook of Chemistry and Physics, CRC Press, Boca Raton, FL, 2005.
46. I.L. Muller, J.R. Galvele, Corros. Sci. 17 (1977) 995–1007.
47. M. Yasuda, F. Weinberg, D. Tromans, J. Electrochem. Soc. 137 (1990) 3708–3715.
48. I.M. Comotti, M. Trueba, S.P. Trasatti, Surf. Interface Anal. 45 (2013) 1575–1584.
49. K.L. Moore, J.M. Sykes, P.S. Grant, Corros. Sci. 50 (2008) 3233–3240.
50. F. Øvari, L. Tomcsanyi, T. Turmezey, Electrochim. Acta. 33 (1988) 323–326.
51. B.E. Wilde, E. Williams, Electrochim. Acta. 16 (1971) 1971–1985
53. B.E. Wilde, Corrosion. 28 (1972) 283–291.
54. G.S. Frankel, J. Electrochem. Soc. 145 (1998) 2186–2198.
55. S.T. Pride, J.R. Scully, J.L. Hudson, J. Electrochem. Soc. 141 (1994) 3028–3040.
56. R.C. Newman, Corros. Sci. 37 (1995) 527–533.
57. K. Nisancioglu, H. Holtan, Corros. Sci. 18 (1978) 1011–1023.
58. R.A. Bonewitz, Corrosion. 30 (1974) 53–59.
59. M. Baumgartner, H. Kaesche, Werkstoffe Und Korrosion. 39 (1988) 129–135.
60. T.R. Beck, Corrosion. 33 (1977) 9–13.
61. T.R. Beck, Electrochim. Acta. 29 (1984) 485–491.
62. G.S. Frankel, S. Fajardo, B.M. Lynch, Faraday Discuss. 180 (2015) 11–33.
63. J.R. Galvele, Corros. Sci. 47 (2005) 3053–3067.
64. E.C. Hornus, C.M. Giordano, M. a. Rodríguez, R.M. Carranza, R.B. Rebak, J. Electrochem. Soc. 162 (2015) C105–C113.
65. K.P. Wong, R.C. Alkire, J. Electrochem. Soc. 137 (1990) 3010–3015.
66. A. Alavi, R.A. Cottis, Corros. Sci. 27 (1987) 443–451.
67. D.W. Siitari, R.C. Alkire, J. Electrochem. Soc. 129 (1982) 481–487.
68. T. Hagyard, J.R. Santhiapillai, J. Appl. Chem. 9 (1959) 323–330.
69. I.L. Rosenfeld, I.K. Marshakov, Corrosion. 20 (1964) 115t–125t.
70. M. Schneider, K. Nocke, H. Worch, Mater. Corros. 51 (2000) 545–551
71. D. D. Macdonald, Corrosion 48 (1992), 194–205.
72. F. Lockwood, S. Lee, J. Faunce, J.A.S. Green, W.J. Ptashnick, Appl. Surf. Sci. 20 (1985) 339–346.
73. N. Birbilis, R.G. Buchheit, J. Electrochem. Soc. 155 (2008) C117–C126.
74. R.P. Hammond, D.M. Eissenberg, D.K. Emmermann, J.E. Jones, H.H. Sephton, F.C. Standiford, R.F. Scott, W.J. Rider, D.W. Dean, Desalination. 99 (1994) 459–481.
74. Hammond, R. P. *et al.* Seawater desalination plant for Southern California. *Desalination* **99,** 459–481 (1994).

## FIGURE CAPTIONS

**Figure 1**. Aluminum specimen (center), rubber O-rings and titanium bolt, nut and washers used for assembling creviced specimens.

**Figure 2.** Cyclic potentiodynamic scans for AA 5052 in 65,000 ppm NaCl at 30°C, in specimens without crevice former, showing the effect of maximum applied current during the forward scan, 250 mA, 45 mA, 3 mA or 0.5 mA, on characteristic potentials.

**Figure 3.** Effect of charge density circulated during cyclic potentiodynamic scans for AA 5052 in 65,000 ppm NaCl at 30°C, in specimens without crevice formers, on $E_{ptp}$ and $E_{r,pit}$. $E_{pit}$ values are included for reference.

**Figure 4.** Cyclic polarization curves of AA 5052, with and without crevice former, in 65,000 ppm NaCl solution at 60°C. Results show similar breakdown and repassivation potentials between creviced and non-creviced specimens.

**Figure 5.** Breakdown and repassivation potentials obtained in experiments (maximum anodic current = 3 mA) with and without crevice formers in 65,000 ppm NaCl, and $E_{corr}$ measured in saturated $AlCl_3$ (with no crevice formers). $E_{corr}$ values measured in deaerated 65000 ppm NaCl and aerated 65000 ppm NaCl + 5 ppm $Cu^{++}$ correspond to specimens with crevice formers. Trend lines are added as visual aid. The presence of the crevice former did not affect the breakdown potentials ($E_{pit}$ and $E_{crev}$) significantly for the three temperatures studied. Vertical hatched bars represent the variation in $E_{corr}$ experienced by the specimens during a 72 h immersion in deaerated 65000 ppm NaCl.

**Figure 6.** Micrographs of AA 5052 after conducting cyclic potentiodynamic polarization experiments with crevice formers, at (from left to right) 30, 60 and 85°C. The white arrow shows the boundary between the crevice former gasket and the electrolyte.
**Figure 7.** Micrographs of AA 5052 under gasket corroded specimen after conducting cyclic potentiodynamic polarization experiments with crevice formers, at (from left to right) 30, 60 and 85°C. Magnifications at the points indicated by the arrows in Figure 6.
**Figure 8.** Evolution of $E_{corr}$ with time (left) and polarization curves (right) of AA 5052 in saturated $AlCl_3$ solution at three temperatures.
**Figure 9.** Scanning electron micrograph of the specimen exposed to 65,000 ppm aerated NaCl with 5 ppm $Cu^{++}$ at 60 °C at $E_{corr}$. Magnification increases from left to right, showing details of the trench formed at the O-ring occluded surface, as indicated by the white square.

***Tables***

**Table 1.** AA 5052 Nominal Chemical Composition (in wt.%).

| Al | Mg | Cr | Cu | Fe | Mn | Si | Zn | Others |
|---|---|---|---|---|---|---|---|---|
| Bal. | 2.2-2.8 | 0.15-0.35 | Max 0.1 | Max 0.4 | Max 0.1 | Max 0.25 | Max 0.1 | Max 0.15 |

***Figures***

**Figure 1**. Aluminum specimen (center), rubber O-rings and titanium bolt, nut and washers used for assembling creviced specimens.

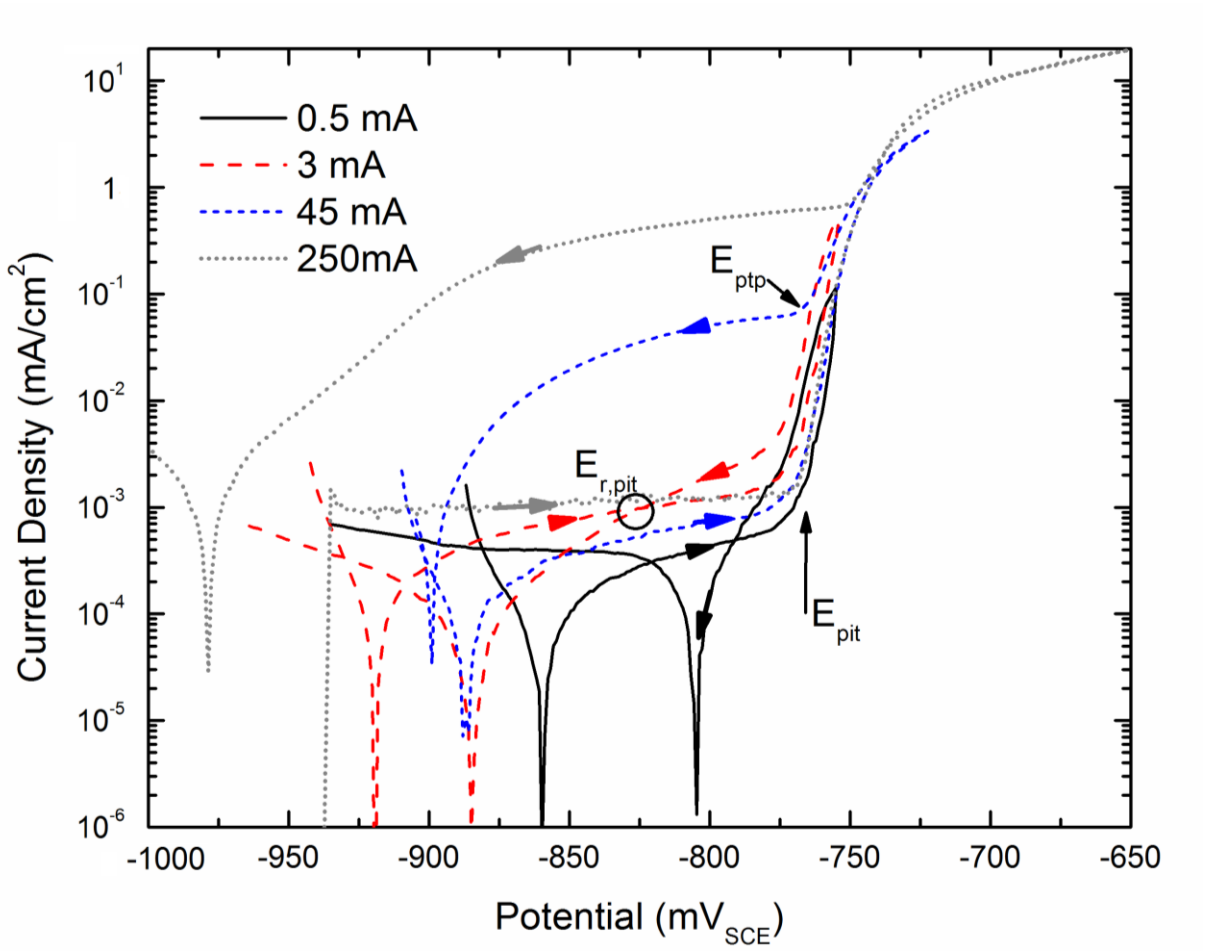


**Figure 2.** Cyclic potentiodynamic scans for AA 5052 in 65,000 ppm NaCl at 30°C, in specimens without crevice former, showing the effect of maximum applied current during the forward scan, 250 mA, 45 mA, 3 mA or 0.5 mA, on characteristic potentials.

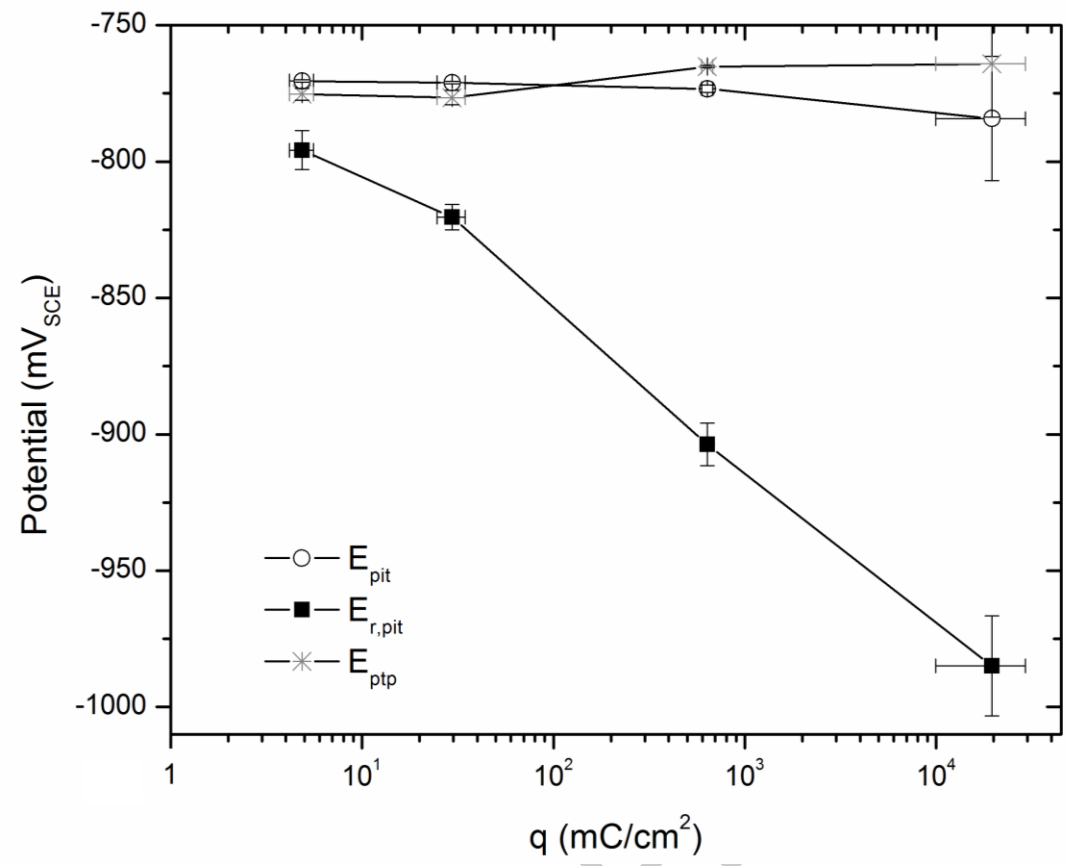


**Figure 3.** Effect of charge density circulated during cyclic potentiodynamic scans for AA 5052 in 65,000 ppm NaCl at 30°C, in specimens without crevice formers, on $E_{ptp}$ and $E_{r,pit}$. $E_{pit}$ values are included for reference. Lines added as visual aid.

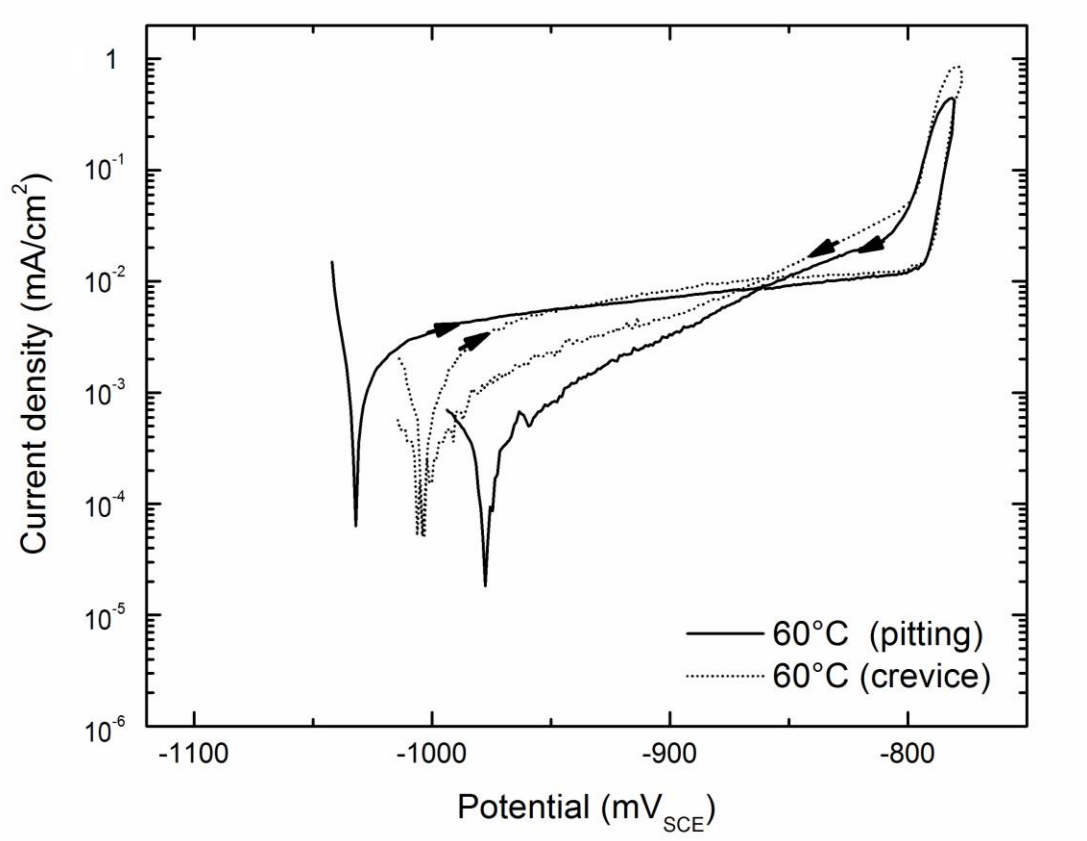


**Figure 4.** Cyclic polarization curves of AA 5052, with and without crevice former, in 65,000 ppm NaCl solution at 60°C. Results show similar breakdown and repassivation potentials between creviced and non-creviced specimens.

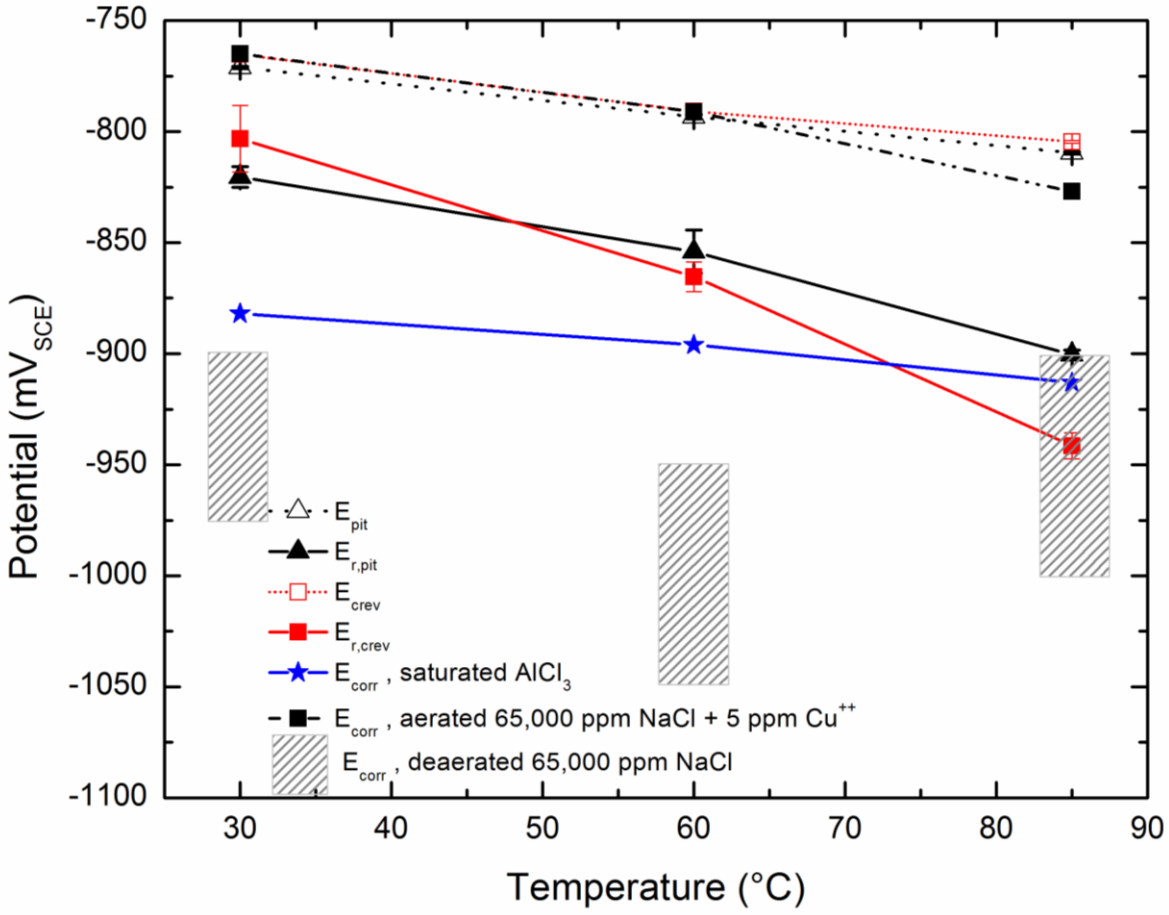


**Figure 5.** Breakdown and repassivation potentials obtained in experiments (maximum anodic current = 3 mA) with and without crevice formers in 65,000 ppm NaCl, and $E_{corr}$ measured in saturated $AlCl_3$ (with no crevice formers). $E_{corr}$ values measured in deaerated 65000 ppm NaCl and aerated 65000 ppm NaCl + 5 ppm $Cu^{++}$ correspond to specimens with crevice formers. Trend lines were added as visual aid. The presence of the crevice former did not affect the breakdown potentials ($E_{pit}$ and $E_{crev}$) significantly for the three temperatures studied. Vertical hatched bars represent the variation in $E_{corr}$ experienced by the specimens during a 72 h immersion in deaerated 65000 ppm NaCl.

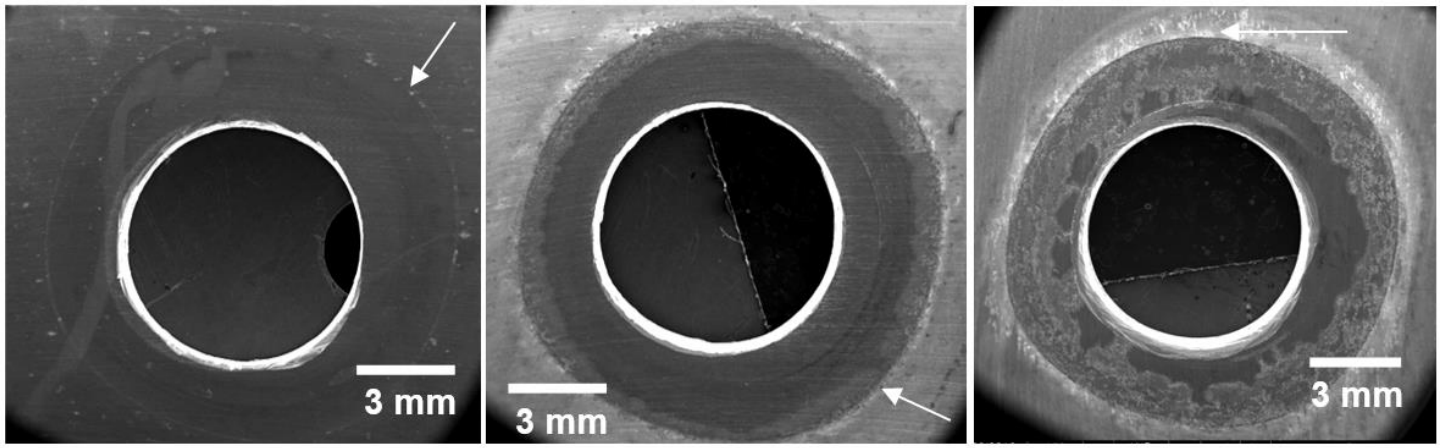


**Figure 6.** Micrographs of AA 5052 after conducting cyclic potentiodynamic polarization experiments with crevice formers, at (from left to right) 30, 60 and 85°C. The white arrow shows the boundary between the crevice former gasket and the electrolyte.

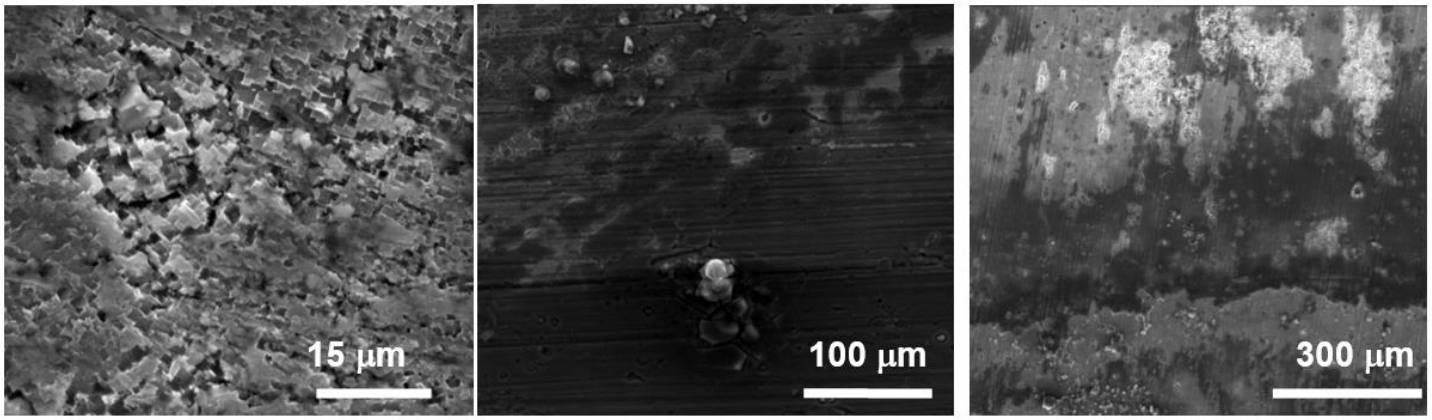


**Figure 7.** Micrographs of AA 5052 under gasket corroded specimen after conducting cyclic potentiodynamic polarization experiments with crevice formers, at (from left to right) 30, 60 and 85°C. Magnifications at the points indicated by the arrows in Figure 6.

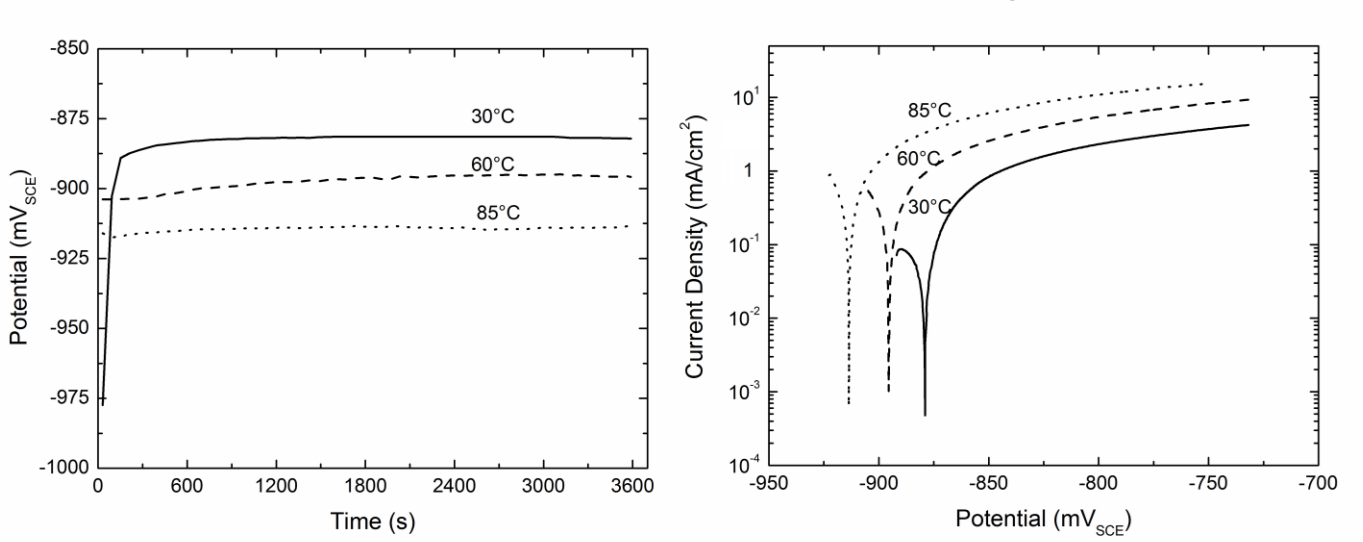


**Figure 8.** Evolution of $E_{corr}$ with time (left) and polarization curves (right) of AA 5052 in saturated $AlCl_3$ solution at three temperatures.

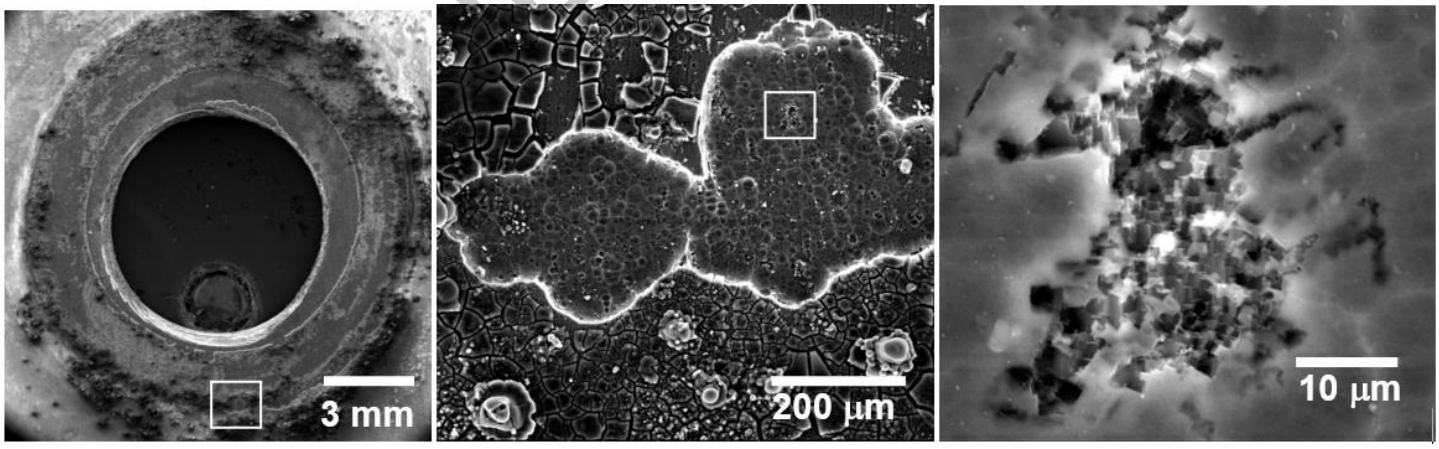


**Figure 9.** Scanning electron micrograph of the specimen exposed to 65,000 ppm aerated NaCl with 5 ppm $Cu^{++}$ at 60 °C at $E_{corr}$. Magnification increases from left to right, showing details of the trench formed at the O-ring occluded surface, as indicated by the white square.